A theoretical asperity contact creep model of interfacial friction for geomaterials

Wurui Ta[1, 2], Runyu Ding[1, 2, #], Fanyu Zhang[1, 2, *]

[1]College of Civil Engineering and Mechanics, Lanzhou University, Lanzhou 730000, China

[2]Key Laboratory of Mechanics on Environment and Disaster in Western China, The Ministry of Education of China, Lanzhou University, Lanzhou 730000, China

[#] Runyu Ding and Wurui Ta contributed equally to this work.

[*] Corresponding author: zhangfy@lzu.edu.cn

Classification: Physical Sciences/Earth Sciences; Physical Sciences/Engineering

Keywords: multiscale interfacial friction model, mechanical-thermo-hydro process, creep cumulation, catastrophic failure, geomaterials

Abstract

How to reveal the physical mechanism affecting the contact and friction behavior of geomaterials is still a challenging problem in predicting geological disasters, such as landslides and earthquakes. In this study, a multiscale friction model is developed to describe the microscopic creep behavior of asperities and the macroscopic sliding friction behavior of geomaterial. The theoretical asperities contact creep model can successfully capture the transition from the mechanical properties of microscopic asperities to the macroscopic interface friction-slip behavior by characterizing the

random contact process of the interface friction through porosity. This model also verifies that the friction behavior of the geomaterials is strongly depends on their temperature, activation energy, and saturation. Thus, the developed model can provide a theoretical basis for a better understanding of the mechanical mechanism of the contact and friction behavior in the geomaterials. Meanwhile, it would be of great help in quantitatively predicting future geological disasters.

Significance statement

Friction was once old, is a new topic again. It is crucial in predicting catastrophic geophysical risks. Thus, a physics-driven model of interfacial friction for geomaterials is developed. This model characterizes the random contact process of the interface through porosity, which successfully captures the transition of mechanical behavior from microscopic asperities to the macroscopic friction interface. Meanwhile, our model finds a close link between velocity-dependent friction versus geomaterial properties and their stress states; and the velocity-dependent friction strengthening or weakening effects are due to differences in directional and tangential activation energy. The proposed mode offers a theoretical explanation for affecting the contact and friction behavior of the geomaterials, which provides a theoretical basis for further prediction of geological disasters.

1. Introduction

In landslides and earthquakes, the geomaterials cause friction and slide due to

unbalanced forces, which can cause serious geological disasters. A description of the interfacial friction behaviors of the geomaterials would be of considerable help in predicting catastrophic failure progress. Considering that the geomaterials possess porous randomness and multiphase heterogeneity, it remains challenging to characterize the interfacial contact process and reveal the friction mechanism of the geomaterials. Nowdays, the predictions of geological disasters mainly focus on empirical or semi-empirical methods deriving from the various real-time monitoring data on displacement and physical parameters of the geomaterials. However, the prediction of geological failure progresses based on physical mechanisms is still an urgent problem to be overcome.

Existing experimental studies focus on the relationship between the friction behavior and sliding velocity of the fault geomaterials (Dieterich, 1978; Marone, 1998; Tsutsumi and Shimamoto, 1997; Scholz and Engelder, 1976; Kilgore *et al.*, 1993), and widely consider the effects of temperature and saturation (Scholz, 2019; Blanpied *et al.*, 1995; Blanpied *et al.*, 1998; Kubo and Katayama, 2015; Morrow *et al.*, 2000). Scholz and Engelder (1976) reported a logarithmic velocity dependence of friction coefficient in sliding experiments of granite. Then, Dieterich (1978) and Michael L. Blanpied et al. (1998) observed similar phenomena on Wsterly granite. They pointed out that granite had inherent velocity-dependent frictional weakening and temperature-dependent frictional strengthening at all velocities. Also, the velocity-dependent frictional weakening is very prevalent in rock avalanches (Hu et al., 2018; Wang et al., 2018; Hu et al., 2022) and glacier avalanches (Iverson *et al.*, 2017; Thøgersen *et al.*, 2019; Gräff

and Walter, 2021), even some flow slides (Wang *et al.*, 2014; Pei *et al.*, 2017). In addition, velocity-dependent frictional strengthening has been observed in the clayed sliding zone of landslides (Wang *et al.*, 2010; Schulz and Wang, 2014; Miao and Wang, 2021). The velocity-dependent friction behavior controls the dynamics of faults and landslides on earth and other planets. These researches have provided new insights into the macro- or micro-mechanisms of the failure progress and velocity-dependent behaviors of geomaterials. Nevertheless, we know little about the underlying physics controlling the velocity-dependent friction behaviors of the geomaterials. Thus, it is urgent to establish a theoretical friction model based on the physical nature of the geomaterials.

Most experimental data-driven theoretical models are semi-empirical formulas lacking physical universality (Dieterich, 1979; Ruina, 1983; Scholz, 1998). Bowden and Tabor (B&T) considered the frictional strength of an interface as the product of an average velocity-dependent contact strength and the ratio of the actual contact area to the total contact area (Bowden and Tabor,1964; Berthoud *et al.*, 1999). The largely empirical rate-and-state (R/S) friction equations and Aging formulation (Dieterich, 1979; Dieterich, 1972) have been widely used to model time-varying friction phenomenology in rock (Marone, 1998; Dieterich, 1979; Beeler *et al.*, 1994) and a diverse set of industrial materials (Berthoud *et al.*, 1999; Prakash, 1998; Ronsin and Coeyrehourcq, 2001; Shroff *et al.*, 2014; Heslot *et al.*, 1994; Carlson and Batista, 1996). Einat Aharonov et al. (2018) developed a microphysics-based creep model, calculating the velocity and temperature dependence of contact stresses during sliding. Their model

89 also focused on the thermal effects of shear heating. Recently, Casper Pranger et al.
90 (2022) proposed transient viscous rheology that produces shear bands that closely
91 mimic the rate- and state- dependent sliding behavior of equivalent fault interfaces.

92 The above theories successfully explain the effect of sliding on friction, especially
93 in a high-velocity sliding state. Most models come from further developments of B&T
94 theory or R/S theory. However, these models are not deep enough to reveal the physical
95 nature of contact and friction behavior of geomaterials. Thus, some parameters of these
96 models remain empirically fitted. The above models do not consider how the
97 deformation of single contact asperities transitions to the entire contact surface because
98 they ignore the stochastic processes of contact and friction. The shear and normal stress
99 are the averages of a contact interface in the models. Moreover, some key influences,
100 such as porosity and permeability, on the friction behavior of geomaterials are still not
101 considered in these models. So, these empirically fitted models are limitations to predict
102 interfacial friction behaviors for geomaterials accurately.

103 On this basis, there is an urgent need to establish a physics-based interfacial
104 friction model coupling micro-contact to macro-friction, which further discloses the
105 effect mechanism of multi-physical factors on the friction behavior of geomaterials. In
106 this study, we develop a multiscale friction model that can describe microscopic contact
107 creep and macroscopic velocity-dependent friction. Then this model is explored to
108 examine the effects of slip velocity, temperature, porosity, and permeability on the
109 frictional behavior of geomaterials. Finally, the physical mechanisms of these
110 influences are discussed. Our model can elucidate the physics of interfacial friction for

111 geomaterials and has the potential to predict geological disaster progresses.

112

113 2. Theoretical model

114 The fiction behavior of geomaterials is considered to be the random and
115 continuous contact of microscopic asperities, resulting in the accumulation of contact
116 deformation and friction, which eventually develops into the sliding of the rough
117 contact surface. Therefore, the theoretical part includes the characterization of the
118 random contact process of the contact surface, the deformation mode of the contacting
119 asperities, and the friction-slip behavior of the rough contact surface.

120 2.1. Characterization of Random Contact Processes

121 Due to the porous nature of geomaterials, the porosity α is used to describe the
122 random contact process on rough surfaces, as shown in Fig. 1. Therefore, the contact
123 between two rough surfaces is considered as a process in which the pore volume is
124 continuously reduced and the real contact area is continuously increased until the
125 porosity is zero. The increase in the real contact area is caused by the continuous
126 increase of the contacting asperities, so a parameter γ is introduced to represent the
127 true contact ratio, which can be expressed as $\gamma = n / N_{\max}$, where n is the number of
128 asperities in contact, $N_{\max}$ is the number of contact asperities after full contact. The
129 porosity in initial contact is α_0, and the γ is considered to be zero at this time. As
130 contact occurs, α gradually decreases to 0, and γ gradually increases to 1.
131 Therefore, the relationship between α and γ can be described by an exponential
132 function

$$\gamma = \begin{cases} A^{\alpha},\ 0 < A < 1,\ 0 \le \alpha < \alpha_0 \\ 0, \quad \alpha = \alpha_0 \end{cases}, \tag{1}$$

where, A is a fitting parameter that can be determined experimentally. The complex random contact process is now characterized by a piecewise exponential function.

2.2 Deformation and friction-slip behavior of the rough contact surface

Sliding of geomaterials is a process of slow accumulation of internal contact and friction, which is consistent with creep characteristics. Therefore, we still describe the deformation of single contacting asperities based on the velocity creep theory proposed by E. Aharonov and C H. Scholz (2018), as follows

$$\sigma_c = \sigma_c^{\,0}[1 - b' \ln(1 + \frac{2r_0}{Vt_c})], \tag{2}$$

$$\tau_c = \tau_c^{*}[1 + a' \ln(\frac{V}{V_{s\max}})], \tag{3}$$

$$T_c = T_0 + \frac{\tau_c}{\rho C}\sqrt{\frac{V}{\pi\beta}}[\sqrt{2\mathrm{r}_0} + \frac{\sigma_n}{\sigma_c}\sqrt{D_{th}}], \tag{4}$$

where, σ_c and τ_c are normal and tangential stresses on the contact asperities interface. T_c is the contact temperature. All parameters included in the equation are shown in Table 1. Equations (2)-(4) illustrate that the deformation of contact asperities is a creep process that is related to temperature, creep activation energy, and creep velocity. Further, the frictional force between individual contacting asperities can be expressed as $F_{si} = \tau_c S_{ri}$, where S_{ri} is the real contact area between individual contacting asperities.

The pressure on single contacting asperities is certain, which satisfies

$\sigma_c S_{ri} = \sigma_n S_i$, where S_i is the nominal contact area of a single asperity and σ_n is the normal stress acting on this nominal contact area. In addition, the sum of the nominal contact areas ($N_{\max} S_i$) of all contacting asperities is equal to the nominal contact area (S_n) of the entire contact surface at the time of full contact, i.e., $N_{\max} S_i = S_n$. Then, F_{si} can be further expressed as

$$F_{si} = \tau_c S_{ri} = \tau_c S_i \frac{\sigma_n}{\sigma_c} = \frac{1}{N_{\max}} S_n \sigma_n \frac{\tau_c}{\sigma_c}. \quad (5)$$

The frictional force F_s at the rough contact surface can be thought of as equal to the sum of the shear forces of each asperity (nF_{si}), as follows

$$F_s = nF_{si} = \frac{n}{N_{\max}} S_n \sigma_n \frac{\tau_c^*[1 + a' \ln(\frac{V}{V_{s\max}})]}{\sigma_c^0[1 - b' \ln(1 + \frac{2r_0}{Vt_c})]} = A^\alpha S_n \sigma_n \frac{\tau_c^*[1 + a' \ln(\frac{V}{V_{s\max}})]}{\sigma_c^0[1 - b' \ln(1 + \frac{2r_0}{Vt_c})]}. \quad (6)$$

The friction coefficient μ_s of the rough contact surface can be defined as the friction force F_s divided by the positive pressure P i.e. $\mu_s = F_s / P$, where positive pressure equals to $S_n \sigma_n$. Therefore, the μ_s can be expressed as

$$\mu_s = \frac{F_s}{P} = A^\alpha \frac{\tau_c^*[1 + a' \ln(\frac{V}{V_{s\max}})]}{\sigma_c^0[1 - b' \ln(1 + \frac{2r_0}{Vt_c})]}. \quad (7)$$

Equation (7) includes porosity α, which is an inherent structural property of the geomaterials. Their pores are closely related to the seepage coefficient and fluid viscosity, which are important factors affecting the friction-slip behavior. Based on the hydraulic diffusivity D_{hyd} ($D_{hyd} = \frac{k}{\eta m}$) (Wibberley, 2002) and the specific storage capacity m ($m = \alpha(c_f + c_{pp})$) (Renner and Steeb, 2014), we can obtain the expression

for the porosity as follows

$$\alpha = \frac{k}{\eta(c_f + c_{pp})D_{hyd}}, \tag{8}$$

where, k is the permeability, η is the fluid viscosity, m is the specific storage capacity, c_f is the compressibility of the pore fluid, and c_{pp} is the compressibility of the pore space. Substituting equation (8) into equation (7), the friction coefficient can be expressed as

$$\mu_s = A^{\frac{k}{\eta(c_f + c_{pp})D_{hyd}}} \frac{\tau_c^*[1 + a' \ln(\frac{V}{V_{s\max}})]}{\sigma_c^0[1 - b' \ln(1 + \frac{2r_0}{Vt_c})]}. \tag{9}$$

Further, based on the relationship between permeability coefficient and saturation $K = Le^{UW_S}$ (K: hydraulic conductivity; W_S: degree of saturation; L, U: fitting parameters) (Li , 2021), the friction coefficient μ_s can be expressed as

$$\mu_s = A^{\frac{Le^{UW_S}}{\rho_f g(c_f + c_{pp})D_{hyd}}} \frac{\tau_c^*[1 + a' \ln(\frac{V}{V_{s\max}})]}{\sigma_c^0[1 - b' \ln(1 + \frac{2r_0}{Vt_c})]} \tag{10}$$

Equation (10) describes the friction coefficient of the macroscopic rough contact surface, which is based on the creep accumulation of microscopic asperities and includes random contact processes. Previous models considered the normal stress (or shear stress) to be the same across the entire contact surface, which was an average treatment. It should be noted especially that equation (10) only considers that the deformation mode of each micro-contact asperity is the same, but the number of contact asperities is random (in accordance with the exponential relationship), which is closer to the real situation.

3. Experimental verification

To validate the proposed model, we compare with the results from high velocity-dependent ring shear tests of a loess landslide at different saturation (Pei *et al.*, 2017), as well as high velocity rotary shear frictional tests of familiar fault geomaterials concerning in quartz sandstone (Dieterich, 1978), granite (Dieterich, 1978; Di Toro *et al.*, 2004) , novaculite (Di Toro *et al.*, 2004; Di Toro *et al.*, 2011).

Figure 2 compares the predicted velocity effect results with the experimental results of loess at different saturation and fault geomaterials at different lithologies in a wide velocity range. The model well captures the velocity weakening effect at close saturation and saturation of loess materials. The experiment shows that for wet loess with saturation higher than 0.8 (0.83, 0.941 and 0.995), its velocity effect is obvious, which is well revealed by the proposed theoretical model (figure 2a). The dry loess, i.e., its saturation is zero, there is no observed velocity-dependent friction effects, and the proposed model can only predict its almost friction-constant behaviors at slide velocity lower 10^{-2} m/s (Figure 2a). The proposed model can also well predict the friction behavior of all compared fault geomaterials involving granite, quartz sandstone, and dense quartzite (Figure 2b). Generally, granite is denser with less porous than quartz and novaculite, which brings about different velocity effects for other fault geomaterials.

We also compare the results from Aharonov and Scholʼs model (Aharonov and Scholz, 2018), which employs the averaging stress at the contact surface. This means that the porosity of the geomaterial is zero, which does not exist in nature. However, the new model considers the influence of temperature and velocity for geomaterials

with different porosity (Figure 2c). It also precisely emerges the three modes and its zones, i.e., no thermal effects, thermal effects, and melting, of contact temperature with increasing slide velocity (Figure 2d). These have entirely consistent with Aharonov and Schol's model (Aharonov and Scholz, 2018).

Therefore, the above results show the validity and correctness of the proposed model. This also indicates that the contact temperature gradually increases until it accumulates to a very high value during the slow sliding process (Zhang *et al.*, 2018). The high temperature further causes the phase transition of the geomaterials, in turn which results in a sharp decrease in the friction coefficient (Figure 2d). The coefficient of friction decreases with increasing saturation in loess, as the water in the pores is subject to pore pressure, which results in a lower friction due to the reduction of the normal force between the contacting asperities. In addition, the liquid also has a lubricating effect. Fault geomaterials with smaller pores have greater internal friction, which means that the actual contact area of the contact surface is bigger thus increasing the tangential force of the contact surface. Therefore, the coefficient of friction decreases with increasing porosity (Figure 2c).

4. Results

4.1 Effect of temperature

The interface temperature of the geomaterial varies with the accumulation of the creep process and the sliding velocity variation. This further affects the frictional behavior of the geomaterial via changing its state. Figures 3 (a) and (b) show the friction

coefficient as a function of contact temperature. The friction coefficient gradually decreases with the increase in contact temperature; meanwhile, it drops sharply when the geomaterial reaches phase transition temperature (e.g. 1850ºC for loess and1670 ºC for geomaterial). This is because temperature affects the normal and tangential creep processes, and has a more significant impact on the tangential direction once a tangential slip occurs. Particularly, the tangential stress decreases with a faster speed than the normal stress as contact temperature increases, causing a decrease in the coefficient of friction. In addition, the geomaterials exhibit obvious flow characteristics before the phase transition temperature.

Figures 3 (c) and (d) show the relationship between the ambient temperature and friction coefficient of the loess and fault geomaterials under different sliding velocities. The influence of ambient temperature on the friction coefficient is smaller than that of the contact temperature because the maximum temperature difference between winter and summer is only tens of degrees Fahrenheit. The ambient temperature change still affects the creep stress in the normal and tangential directions of these geomaterials, thus, the friction coefficient gradually decreases with the increase in temperature.

4.2 Strengthening and weakening effects of friction

Before the contact temperature reaches the phase transition temperature, the friction coefficient will show different trends with the increase of sliding velocity, i.e., gradually decreasing (weakening effect), basically unchanged, and progressively increasing (strengthening effect). This is since the difference between the creep

activation energy in the normal and tangential directions of the geomaterial.

This difference indicates the relative ease with which creep occurs in the normal and tangential directions. When the difference between the activation energy of tangential and normal creep is small, the friction coefficient is a very slight change with the slow increase of the sliding velocity. This means that the tangential and normal creep processes are similar in difficulty, resulting in almost constant friction coefficient, as shown in Figure 4.

When the creep activation energy in the normal direction of the asperities is smaller than that in the tangential direction, the friction coefficient decreases gradually with the slow increase of the sliding velocity (Figure 4). This is because normal creep is more likely to occur, and the normal stress reduction is smaller than the tangential stress reduction. As a result, the friction coefficient decreases. Similarly, when the creep activation energy in the normal direction of the asperities is greater than that in the tangential direction, the friction coefficient gradually increases with the slow increase of the sliding velocity (Figure 4). This is because tangential creep is more likely to occur and the tangential stress reduction is smaller than the normal stress reduction, causing an increase in the coefficient of friction.

The creep activation energy of geomaterials is closely related to the properties, composition, and other factors of these geomaterials. Therefore, different materials will show shear strengthening or weakening, even constant shear strength with increasing slide velocity.

4.3. The effect of permeability and viscosity

The permeability coefficient and liquid viscosity can significantly affect the frictional behavior of geomaterials as they determine water distribution and flow characteristics in geological disasters.

Figure 5 shows the effect of permeability coefficient and fluid viscosity on friction coefficient at different velocities. The coefficient of friction decreases as the permeability coefficient increases. This is because the larger permeability makes the water flow more easily and widely in granular materials, such as loess, which enhances the lubrication effect and reduces the force between asperities. Similarly, fluid viscosity can hinder its flow and widespread distribution in granular materials. Therefore, the coefficient of friction increases with the coefficient of fluid viscosity.

The above results elucidate that the macroscopic contact and friction behavior of the geomaterials depend on the creep accumulation process of microscopic asperities in the normal and tangential directions. This is closely related to temperature and creep activation energy. However, temperature-induced changes in normal and tangential stresses and phase transitions significantly affect the changes in its frictional force. The relative creep difference in the normal and tangential directions of the asperities can cause velocity strengthening or weakening effects. It is due to the different amounts of stress reduction in the tangential and normal directions corresponding to different activation energies. In addition, the water content also significantly affects its friction coefficient, which can attribute to the lubrication effect and the role of sharing part of the pore pressure. Thus, the permeability and fluid viscosity coefficients, which affect

300 the water flow and distribution characteristics, affect the coefficient of friction.

301

302 ## 5. Conclusion

303 Based on frictional contact theory, a physics-driven model of interfacial friction is
304 built for geomaterials. Our theoretical model characterizes the random contact process
305 of the interface through porosity, which successfully captures the transition of
306 mechanical behavior from microscopic asperities to the macroscopic friction interface.
307 The theory reveals the velocity-dependent sliding friction behavior of these verified
308 geomaterials and shows that the interparticle contact temperature has a more dominant
309 role in velocity-dependent friction than the ambient temperature. The velocity-
310 dependent friction behavior can attribute to the adjustment of stress state and property
311 during high-velocity shearing. Meanwhile, the difference in directional and tangential
312 activation energy can cause velocity-enhancing or weakening effects for geomaterials.
313 The saturation of geomaterials not only exhibits the lubrication effect but also shares
314 part of the pore pressure, which contribute to the decrease in the friction coefficient.
315 Thus, the permeability and fluid viscosity coefficients, which affect the water flow and
316 distribution characteristics, also affect the coefficient of friction. These findings provide
317 a further understanding of the physical mechanism how shear velocity affect the contact
318 and sliding friction of geomaterials. It has important implications for geological hazard
319 prediction, not only in landslides and earthquakes but also in glacial avalanches on earth,
320 even slide failure progresses on other planets.

321

Conflict of Interest

The authors declare no conflicts of interest relevant to this study.

Acknowledgement

The works are supported by the National Key R&D Program of China (2022YFC3003401), Natural Science Foundation of China (Nos. 12272157 and 42090053), the Fundamental Research Funds for the Central Universities (Nos. lzujbky-2021-55 and lzujbky-2021-ct04).

References

Aharonov, E., & Scholz, C. H. (2018). A physics-based rock friction constitutive law: Steady state friction. *Journal of Geophysical Research: Solid Earth*, *123*(2), 1591-1614. https://doi.org/10.1002/2016JB013829

Beeler, N. M., Tullis, T. E., & Weeks, J. D. (1994). The roles of time and displacement in the evolution effect in rock friction. *Geophysical research letters*, *21*(18), 1987-1990. https://doi.org/10.1029/94GL01599

Berthoud, P., Baumberger, T., G'sell, C., & Hiver, J. M. (1999). Physical analysis of the state-and rate-dependent friction law: Static friction. *Physical Review B*, *59*(22), 14,313–14,327. https://doi.org/10.1103/PhysRevB.59.14313

Blanpied, M. L., Lockner, D. A., & Byerlee, J. D. (1995). Frictional slip of granite at hydrothermal conditions. *Journal of Geophysical Research*, *100*(B7), 13,045–13,064. https://doi.org/10.1029/95JB00862

Blanpied, M. L., Tullis, T. E., & Weeks, J. D. (1998). Effects of slip, slip rate, and shear

heating on the friction of granite. *Journal of Geophysical Research: Solid Earth*, *103*(B1), 489-511. https://doi.org/10.1029/97JB02480

Bowden, F. P., & Tabor, D. (1964). *The friction and lubrication of solids* (Vol. 2, No. 2). Oxford: Clarendon press.

Carlson, J. M., & Batista, A. A. (1996). Constitutive relation for the friction between lubricated surfaces. *Physical Review E*, *53*(4), 4153– 4165. https://doi.org/10.1103/PhysRevE.53.4153

Di Toro, G., Goldsby, D. L., & Tullis, T. E. (2004). Friction falls towards zero in quartz rock as slip velocity approaches seismic rates. *Nature*, *427*(6973), 436–439. https://doi.org/10.1038/nature02249

Di Toro, G., Han, R., Hirose, T., De Paola, N., Nielsen, S., Mizoguchi, K., … Shimamoto, T. (2011). Fault lubrication during earthquakes. *Nature*, *471*(7339), 494–498. https://doi.org/10.1038/nature09838

Dieterich, J. H. (1972). Time-dependent friction in rocks. *Journal of Geophysical Research*, *77*(20), 3690–3697. https://doi.org/10.1029/JB077i020p03690

Dieterich, J. H. (1978). Time-dependent friction and the mechanics of stick-slip. *Pure and Applied Geophysics*, *116*(4-5), 790–806. https://doi.org/10.1007/BF00876539

Dieterich, J. H. (1979). Modeling of rock friction: 1. Experimental results and constitutive equations. *Journal of Geophysical Research*, *84*(B5), 2161–2168. https://doi.org/10.1029/JB084iB05p02161

Gräff, D., Walter, F. (2021). Changing friction at the base of an Alpine glacier. *Scientific Reports 11*, 10872. https://doi.org/10.1038/s41598-021-90176-9

Heslot, F., Baumberger, T., Perrin, B., Caroli, B., & Caroli, C. (1994). Creep, stick-slip, and dry friction dynamics: Experiments and a heuristic model. *Physical Review E*, *49*(6), 4973–4988. https://doi.org/10.1103/PhysRevE.49.4973

Hu, W., Huang, R., McSaveney, M., Zhang, X. H., Yao, L., & Shimamoto, T. (2018). Mineral changes quantify frictional heating during a large low-friction landslide. *Geology*, *46*(3), 223-226. https://doi.org/10.1130/G39662.1

Hu, W., Xu, Q., McSaveney, M., Huang, R., Wang, Y., Chang, C. S., ... & Zheng, Y. (2022). The intrinsic mobility of very dense grain flows. *Earth and Planetary Science Letters*, *580*, 117389. https://doi.org/10.1016/j.epsl.2022.117389

Iverson, N. R., Hooyer, T. S., & Baker, R. W. (1998). Ring-shear studies of till deformation: Coulomb-plastic behavior and distributed strain in glacier beds. *Journal of Glaciology*, *44*(148), 634-642. https://doi.org/10.3189/s0022143000002136

Kilgore, B. D., Blanpied, M. L., & Dieterich, J. H. (1993). Velocity dependent friction of granite over a wide range of conditions. *Geophysical Research Letters*, *20*(10), 903–906. https://doi.org/10.1029/93GL00368

Kubo, T., & Katayama, I. (2015). Effect of temperature on the frictional behavior of smectite and illite. *Journal of Mineralogical and Petrological Sciences*, *110*(6), 293-299. https://doi.org/10.2465/jmps.150421

Li, Y., (2021). Study on Unsaturated Soil Model Based on Soil Water Characteristic Curve. North China University of Water Resources and Electric Power.

Marone, C. (1998). Laboratory-derived Friction Laws and Their Application to Seismic

389 Faulting. *Annual Review of Earth and Planetary Sciences*, *26*(1), 643–696.
390 https://doi.org/10.1146/annurev.earth.26.1.643
391 Miao, H., & Wang, G. (2021). Effects of clay content on the shear behaviors of sliding
392 zone soil originating from muddy interlayers in the Three Gorges Reservoir, China.
393 *Engineering Geology*, *294*, 106380.
394 https://doi.org/10.1016/j.enggeo.2021.106380
395 Morrow, C. A., Moore, D. E., & Lockner, D. A. (2000). The effect of mineral bond
396 strength and adsorbed water on fault gouge frictional strength. *Geophysical*
397 *Research Letters*, *27*(6), 815-818. https://doi.org/10.1029/1999gl008401
398 Pei, X., Zhang, X., Guo, B., Wang, G., & Zhang, F. (2017). Experimental case study of
399 seismically induced loess liquefaction and landslide. *Engineering Geology*, *223*,
400 23-30. https://doi.org/10.1016/j.enggeo.2017.03.016
401 Prakash, V. (1998). Frictional response of sliding interfaces subjected to time varying
402 normal pressures. *Journal of Tribology*, *120*(1), 97– 102.
403 https://doi.org/10.1115/1.2834197
404 Pranger, C., Sanan, P., May, D. A., Le Pourhiet, L., & Gabriel, A.-A. (2022). Rate and
405 state friction as a spatially regularized transient viscous flow law. *Journal of*
406 *Geophysical Research: Solid Earth*, *127*(6), e2021JB023511.
407 https://doi.org/10.1029/2021JB023511
408 Renner, J., & Steeb, H. (2015). Modeling of fluid transport in geothermal research.
409 *Handbook of Geomathematics*, 1443-1500. http://doi.org/10.1007/978-3-642-
410 27793-1_81-2

411 Ronsin, O., & Coeyrehourcq, K. L. (2001). State, rate and temperature–dependent
412 sliding friction of elastomers. *Proceedings of the Royal Society of London. Series*
413 *A: Mathematical, Physical and Engineering Sciences*, *457*(2010), 1277-1294.
414 https://doi.org/10.1098/rspa.2000.0718
415 Ruina, A. (1983). Slip instability and state variable friction laws. *Journal of*
416 *Geophysical Research: Solid Earth*, *88*(B12), 10359-10370.
417 https://doi.org/10.1029/JB088iB12p10359
418 Scholz, C. H. (1998). Earthquakes and friction laws. *Nature*, *391*(6662), 37-42.
419 https://doi.org/10.1038/34097
420 Scholz, C. H. (2019). *The mechanics of earthquakes and faulting*. Cambridge university
421 press.
422 Scholz, C. H., & Engelder, T. (1976). Role of asperity indentation and ploughing in
423 rock friction. *International Journal of Rock Mechanics and Mining Sciences*, *13*(5),
424 149–154. https://doi.org/10.1016/0148-9062(76)90819-6
425 Schulz, W. H., & Wang, G. (2014). Residual shear strength variability as a primary
426 control on movement of landslides reactivated by earthquake-induced ground
427 motion: Implications for coastal Oregon, US. *Journal of Geophysical Research:*
428 *Earth Surface*, *119*(7), 1617-1635. https://doi.org/10.1002/2014jf003088
429 Shroff, S. S., Ansari, N., Robert Ashurst, W., & de Boer, M. P. (2014). Rate-state friction
430 in microelectromechanical systems interfaces: experiment and theory. *Journal of*
431 *Applied Physics*, *116*(24), 244902. https://doi.org/10.1063/1.4904060
432 Thøgersen, K., Gilbert, A., Schuler, T. V., & Malthe-Sørenssen, A. (2019). Rate-and-

433 state friction explains glacier surge propagation. *Nature Communications*, *10*(1),
434 2823. https://doi.org/10.1038/s41467-019-10506-4
435 Tsutsumi, A., & Shimamoto, T. (1997). High-velocity frictional properties of gabbro.
436 *Geophysical Research Letters*, *24*(6), 699-702. https://doi.org/10.1029/97gl00503
437 Wang, G., Suemine, A., & Schulz, W. H. (2010). Shear-rate-dependent strength control
438 on the dynamics of rainfall-triggered landslides, Tokushima Prefecture, Japan.
439 Earth Surface Processes and Landforms, 35(4), 407-416.
440 https://doi.org/10.1002/esp.1937
441 Wang, G., Suemine, A., Zhang, F., Hata, Y., Fukuoka, H., & Kamai, T. (2014). Some
442 fluidized landslides triggered by the 2011 Tohoku earthquake (Mw 9.0), Japan.
443 Geomorphology, 208, 11- 21. https://doi.org/10.1016/j.geomorph.2013.11.009
444 Wang, Y. F., Dong, J. J., & Cheng, Q. G. (2018). Normal stress-dependent frictional
445 weakening of large rock avalanche basal facies: Implications for the rock
446 avalanche volume effect. Journal of Geophysical Research: Solid Earth, 123(4),
447 3270-3282. https://doi.org/10.1002/2018jb015602
448 Wibberley, C. A. J. (2002). Hydraulic diffusivity of fault gouge zones and implications
449 for thermal pressurization during seismic slip. Earth, Planets and Space, 54(11),
450 1153-1171. https://doi.org/10.1186/BF03353317
451 Zhang, F., Kong, R., & Peng, J. (2018). Effects of heating on compositional, structural,
452 and physicochemical properties of loess under laboratory conditions. Applied Clay
453 Science, 152, 259-266. https://doi.org/10.1016/j.clay.2017.11.022

Figures

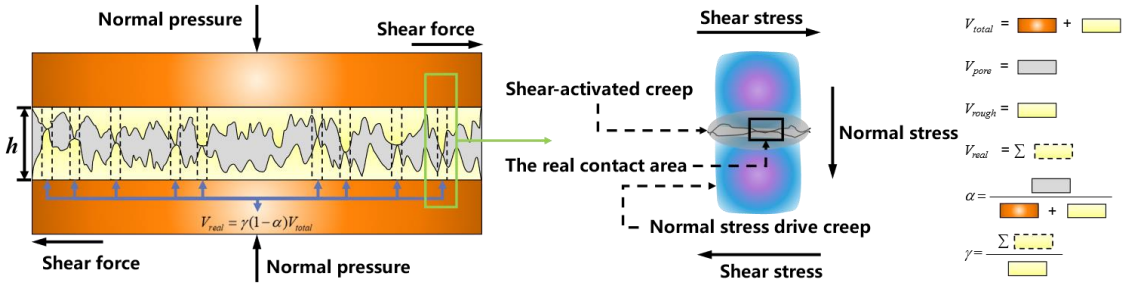

Figure 1. Illustration of the profile of shearing contact rough surface and single contacted asperities. The blue region depicts a highly compressed area that experience internal creep driven by normal stress, with the maximum compressed region is represented by purple. The gray area contains localized shear-activated creep.

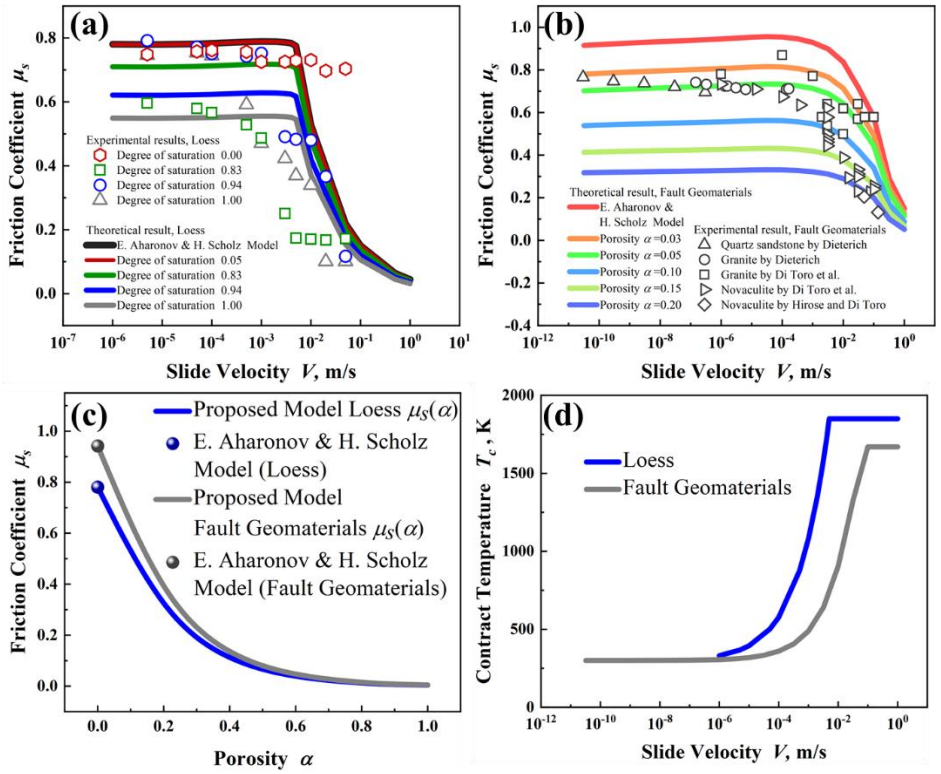

Figure 2. The comparison of the prediction results of the proposed model with the experimental results of loess (a) and fault geomaterials (b). (c) Coefficient of friction as a function of porosity. (d) The relationship between the contact temperature of the contact surface of the geomaterial and the sliding velocity.

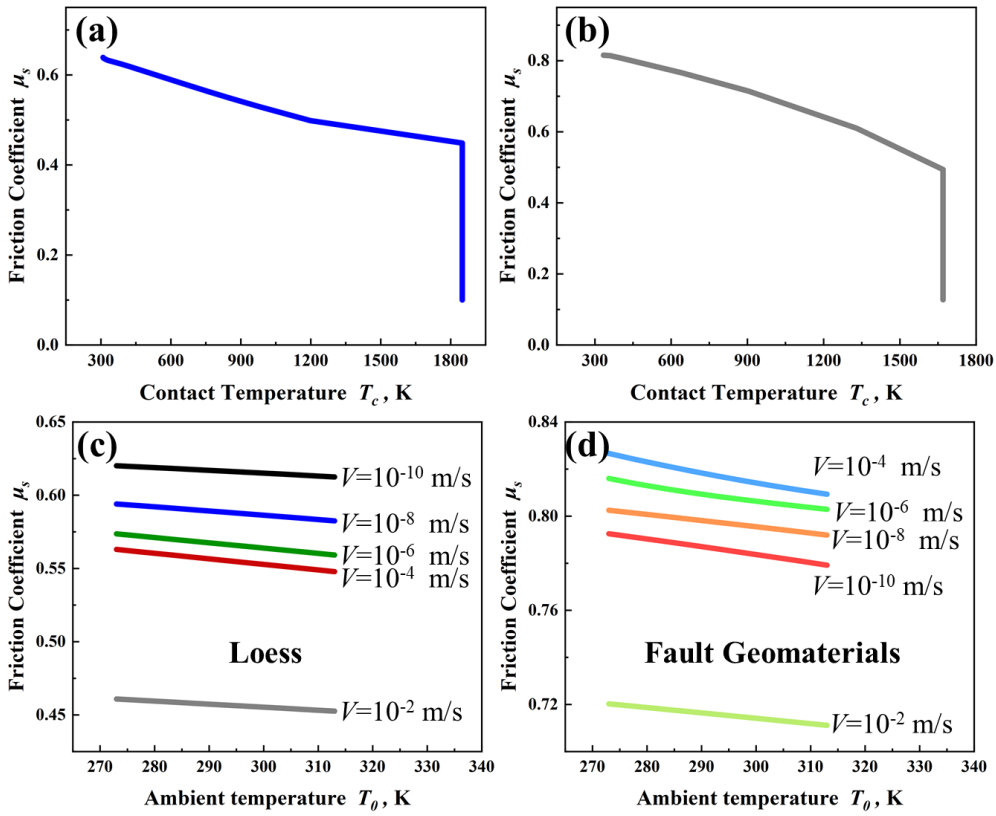

Figure 3. (a) The relationship between the contact temperature of the contact surface and friction coefficient of the loess. (b) The relationship between the contact temperature of the contact surface and friction coefficient of the fault geomaterial. (c) The relationship between the ambient temperature and friction coefficient of the loess under different sliding velocities. (d) The relationship between the ambient temperature and friction coefficient of the fault geomaterial under different sliding velocities.

474

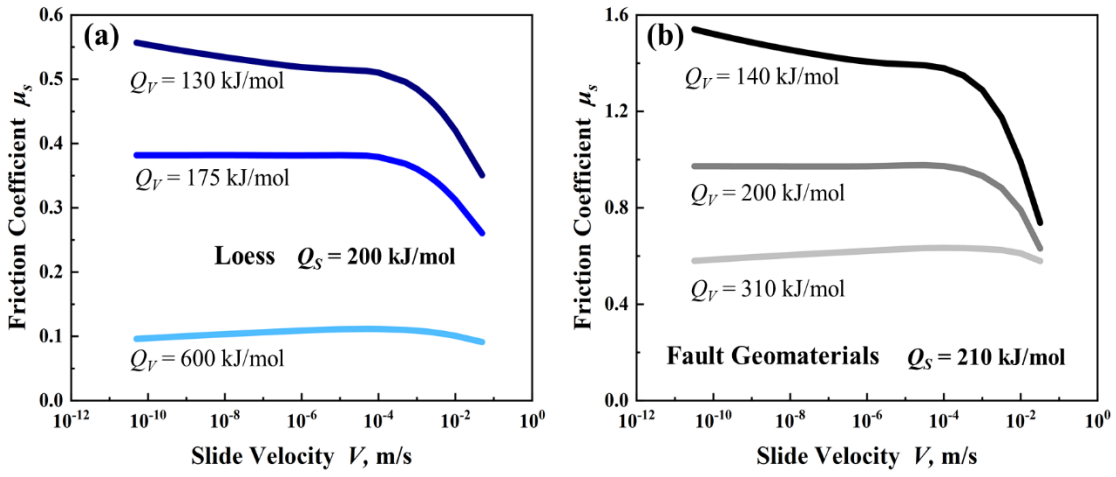

475

476 **Figure 4.** (a) Effect of creep activation energy difference on friction coefficient of loess. (b) Effect

477 of creep activation energy difference on friction coefficient of fault geomaterial.

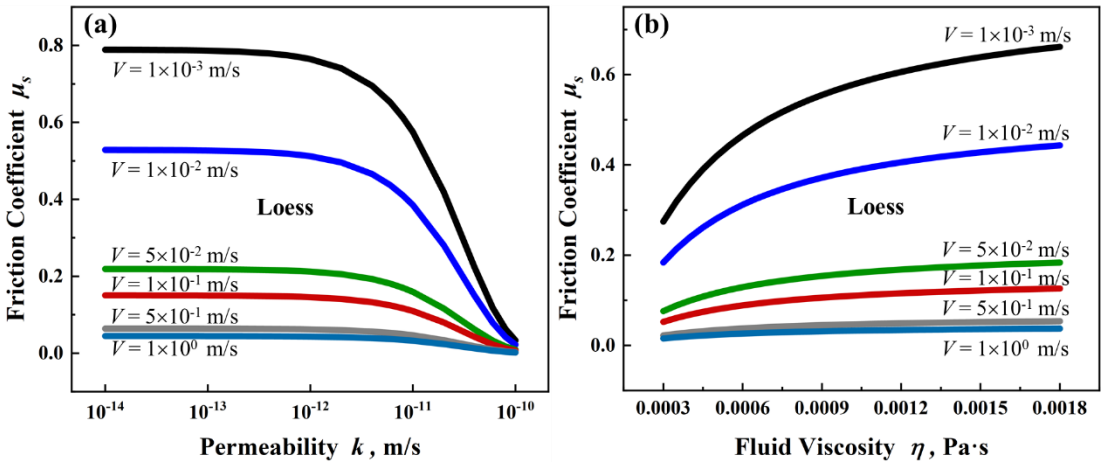

Figure 5. (a) Effect of permeability on friction coefficient of loess. (b) Effect of fluid viscosity on friction coefficient of loess.

Table 1. Table of Parameters, Definitions, and Values

Parameters	Value (Quartz)	Value (Loess)
σ_n^0	$\sigma_c^{\,0} = \frac{Q_V B}{N_A \Omega_v}$	N_A is the Avogadro number
τ_c^*	$\tau_c^{\,*} = \frac{Q_S}{N_A \Omega_S}$	N_A is the Avogadro number
a'	$a' = \frac{RT_c}{Q_S}$	R is the Gas constant
b'	$b' = \frac{RT_c}{Q_V B}$	R is the Gas constant
Q_S (KJ/mol) Surface activation energy	210	660
Q_V (KJ/mol) Volume activation energy	240	400
Ω_S (10^{-29}m^3) Surface activation volume	6.00	3.10
Ω_V (10^{-29}m^3) Volume activation volume	6.80	1.40
B Prefactor	0.8	0.9
r_0 (mm) Contact radius	5	5
t_c (s) Cutoff time	$t_c = t_{cr}\frac{T_c}{T_{cr}}\exp(-\frac{E_{tc}}{RT_c}\frac{\triangle T_c}{T_{cr}})$	$t_c = t_{cr}\frac{T_c}{T_{cr}}\exp(-\frac{E_{tc}}{RT_c}\frac{\triangle T_c}{T_{cr}})$
t_{cr} (s) Reference cutoff time	2	2
T_{cr} (K) Reference temperature	300	300
E_{tc} (KJ/mol) Activation energy for t_c	$E_{tc} = (1-B)Q_V$	$E_{tc} = (1-B)Q_V$
V_{smax} (m/s) Maximum shear rate	1875	200
T_0 (K) Ambient temperature	300	300
C (J/kg/K) Specific Heat Capacity	730*(170-200/T_c)	3000-(300000/T_c)

β (m²/s) Thermal diffusivity	$\beta_0\times10^{-4}/T_c$-0.5×10⁻⁷	$\lambda/(\rho \cdot C)$
β_0(m²/s) Thermal diffusivity	2.5	-
ρ (kg/m³) Density	2650	1400
λ (W/m/K) Heat transfer rate	-	1.2
D_{th} Thermal equilibration distance	$D_{th}=k\sigma_n^{\ q}$ here assume k = 5, q = -1.	$D_{th}=k\sigma_n^{\ q}$ here assume k = 5, q = -1.
σ_n (MPa) Applied normal stress	5	0.2
T_m (K) (Pre) melting temperature	1670	1850
A	0.005	0.005, 0.0005, 0.03, 0.4
D_{hyd} (m²/s) Hydraulic diffusivity	-	0.0008
c_f (kPa⁻¹) Compressibility of the pore space	-	-
c_{pp} (kPa⁻¹) Compressibility of the pore fluid	-	-
c_{pp} + c_f (kPa⁻¹)		3×10⁻⁷
η (Pa·s) Fluid viscosity	-	3×10⁻⁴ ~ 1.8×10⁻³
k (m²) Permeability	-	1×10⁻¹⁴ ~ 1×10⁻¹⁰
K (m/s) Hydraulic conductivity	-	$K=Le^{UW_S}$ E = 2.172×10⁻⁸ , F = 10.55

484